Analytica Chimica Acta 1221 (2022) 340095

Contents lists available at ScienceDirect

Analytica Chimica Acta

journal homepage: www.elsevier.com/locate/aca

Photocurrent quenching by competitive consumption of surface electron donor and light absorption for immunosensing

Yu Du [a,b], Siqi Yu [a], Zhaohui Li [c], Huangxian Ju [a,*]

[a] State Key Laboratory of Analytical Chemistry for Life Science, School of Chemistry and Chemical Engineering, Nanjing University, Nanjing, 210023, China
[b] Collaborative Innovation Center for Green Chemical Manufacturing and Accurate Detection, University of Jinan, Jinan, 250022, China
[c] College of Chemistry, Green Catalysis Center, Henan Joint International Research Laboratory of Green Construction of Functional Molecules and Their Bioanalytical Applications, Zhengzhou University, Zhengzhou, 450001, China

HIGHLIGHTS

- A photocurrent quenching strategy by competitive consumption of surface electron donor and light absorption is proposed.
- The novel strategy has been used for construction of photoelectrochemical immunosensing method.
- ZnSnO3 nanocubes/BiOI nanoarrays/polydopamine as photoactive material shows enhanced sensitive photocurrent signal.
- The proposed method for NSE shows a linear range of 0.1 pg/mL −20 ng/mL and a detection limit of 0.03 pg/mL.

GRAPHICAL ABSTRACT

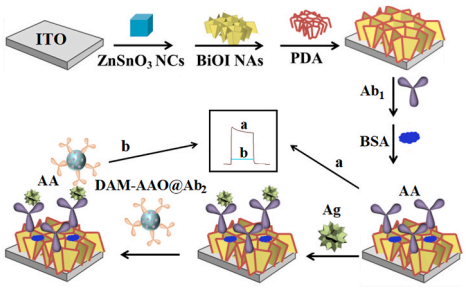

ARTICLE INFO

Keywords:
Photoelectrochemical immunosensors
Photocurrent
Quenching effect
Electron donor
Neuron specific enolase
Labelling immunoassay

ABSTRACT

This work designs a competitive consumption strategy of surface electron donor and light absorption for quenching the photocurrent of $ZnSnO_3$ nanocubes/BiOI nanoarrays/polydopamine ($ZnSnO_3$ NCs/BiOI NAs/PDA) as a photoactive material. This material can be formed on electrode surface by successive coating and deposition to provide a substrate for immobilization of capture antibody, and producing strong photocurrent in the presence of ascorbate acid as a surface electron donor due to the well matching structure of band gaps between $ZnSnO_3$ NCs and BiOI NAs, the excellent light absorption ability and high photo-electron conversion efficiency of BiOI NAs and PDA, and the accelerated electron transfer. Using ascorbate oxidase loaded dopamine-melanin nanosphere (DAM-AAO) as a label of the signal (secondary) antibody, the sandwich-type immunoreaction leads to dual photocurrent quenching of the label through the competitive consumption of ascorbate acid with enzymatic oxidation and the light absorption by DAM nanosphere. Thus, a sensitive "On-Off" photoelectrochemical (PEC) immunosensing method is constructed for the analysis of neuron specific enolase (NSE). The proposed method shows a detection range of 0.1 pg/mL −50 ng/mL and a detection limit of 0.03 pg/mL. The excellent performance and the recovery text demonstrated the practicability of the designed strategy and label in immunoassay of different protein biomarkers.

* Corresponding author.
E-mail address: hxju@nju.edu.cn (H. Ju).

https://doi.org/10.1016/j.aca.2022.340095
Received 9 May 2022; Received in revised form 10 June 2022; Accepted 13 June 2022
Available online 16 June 2022

1. Introduction

Photoelectrochemistry has been widely used for the design of photoelectrochemical (PEC) analytical methods due to its rapid response, high throughput, simple instrument and the development of different photoactive materials [1]. The different energy forms of excitation source (light) and detection signal (current) endow PEC detection with low background and high sensitivity [2,3]. By co-immobilizing photoactive material and capture antibody on electrode surface or babelling the antibody with photoactive material, the PEC immuosensors can be conveniently prepared for immunoassay of target analytes, such as protein biomarkers [4–6]. Moreover, these immuosensors can be combined with controlled-release strategy [7] and multiple signal amplification [8] strategy to further improve the sensitivity and stability of the assay. Obviously, the photoactive materials play major roles in the construction of PEC immunosensors and their performances [9] To produce strong photocurrent signal, the photoactive materials should possess good ability of light absorption, high photo-to-current conversion efficiency, quick charge separation, and less electron-hole recombination, which can generally be achieved by the sensitized structure composed of different semiconductors with matching band gaps [6,10].

As a multifunctional material, zinc stannate ($ZnSnO_3$) has been used in numerous fields, such as photoelectric catalysis, gas sensing and electrochemical nanodevices [11–13]. Compared with ZnO and SnO_2, $ZnSnO_3$ has excellent photoelectric properties and chemical stability under severe conditions. However, its wide band gap results in poor absorption of visible light [14,15], which limits its application in PEC detection of biomolecules. In order to overcome the shortcomings, this work used bismuth oxyiodide (BiOI) with narrow band gap to construct a sensitized structure by successive ion layer adsorption and reaction (SILAR), which formed bismuth oxyiodide nanoarrays (BiOI NAs) on $ZnSnO_3$ nanocubes ($ZnSnO_3$ NCs) and greatly improved the effective area of visible light absorption [16–18]. Thus the sensitized structure could be used for preparation of immunosensors by self-oxidation polymerization of dopamine on its surface [19] to bind the capture antibody (Ab_1). The formed polydopamine (PDA) is a multipurpose material with amazing fuctions in optical, electrical, thermal and magnetic fields [19,20]. Here, the presence of thin PDA film enhenced photo-electron conversion efficiency and accelerated the electron transfer. Thus the $ZnSnO_3$ NCs/BiOI NAs/PDA modified ITO or the prepared immunosensors showed strong photocurrent in the presence of ascorbate acid (AA) as a surface electron donor.

In order to perform the immunoassay, a competitive consumption strategy of the surface electron donor and light absorption was designed for quenching the photocurrent, which was achieved by labelling the secondary antibody (Ab_2) with ascorbate oxidase (AAO) loaded dopamine-melanin nanosphere (DAM NP) [21]. While the AAO catalyzed the oxidation of AA at immunosensor surface after sandwich-type immunoreaction, the simultaneously introduced DAM NPs could absorb the light, and thus further decreased the photocurrent, leading to sensitive "On-Off" immunoassay method for the target antigen. Using neuron-specific enolase (NSE), an enolase that exists in nerve tissues and neuroendocrine tissues and has been used as a biomarker for neuroblastoma and cancer diagnosis [22], as the analyte model, the immunosensor showed a wide concentration range, a low detection limit down to 0.03 pg/mL, stable signal response and good selectivity. The acceptable recovery for the detection of NSE spiked in serum samples demonstrated the practicability of the designed dual quenching strategy and label in immunoassay of different protein biomarkers.

2. Experiments

2.1. Reagents and apparatus

NSE and *anti*-NSE antibody were gained from Biocell Science Co. Ltd., (Shanghai, China). Bovine serum albumin (BSA, 96–99%) and ascorbate oxidase were purchased from Sigma reagent Co., Ltd. (St. Louis, MO, USA). Stannic chloride ($SnCl_4{\cdot}5H_2O$), zinc sulfate heptahydrate ($ZnSO_4{\cdot}7H_2O$) and concentrated ammonia ($NH_3{\cdot}H_2O$) were obtained from Aladdin Reagent Database Inc. (Shanghai, China). Dopamine hydrochloride was purchased from Sinopharm Chemical Reagent Co. Ltd. (Beijing, China). N-hydroxysuccinimide (NHS) and (1-(3-dimethylaminopropyl) -3-ethylcarbodiimide hydrochloride) (EDC) were purchased from Shanghai Civi-Chem Co., Ltd. Phosphate buffered saline (PBS) was prepared using 0.1 mol L^{-1} Na_2HPO_4 and 0.1 mol L^{-1} KH_2PO_4 solution. Ultrapure water was utilized in all experiments.

Scanning electron microscopic (SEM) images and energy dispersive spectra (EDS) were obtained using a field emission SEM (Zeiss, Germany). X-ray diffraction (XRD) patterns were obtained by using D8 focus diffractometer (Bruker AXS, Germany). X-ray photoelectron spectroscopic (XPS) measurements were recorded on a 2000 XPS system with a monochromatic Al Kα source and a charge neutralizer. UV–vis spectra were obtained on a Shimadzu UV-3101PC spectrometer (Japan). Electrochemical impedance spectra (EIS) were examined with a electrochemical workstation (Zahner Zennium PP211, Germany) using $[Fe(CN)_6]^{3-/4-}$ as a couple of redox probes. Indium tin oxide (ITO) (resistivity 10 Ω/sq) glass was obtained from Zhuhai Kaivo Electronic Components Co. Ltd., China. The PEC experiments were carried out on a homemade PEC workstation including a LED lamp (100 W, white light) as an irradiation source and a CHI760E electrochemical workstation (Shanghai Chenhua Instruments Co., Ltd, China).

2.2. Synthesis of $ZnSnO_3$ NCs and DAM NPs

The $ZnSnO_3$ NCs was synthesized according to the previous reported [15]. Typically, 0.16 g $SnCl_4{\cdot}5H_2O$ and 0.07 g NaOH were dispersed in 20 mL ultrapure water. The pH value was controlled to 12.6 by adding NaOH (3 mol/L) solution. Afterward, 0.13 g $ZnSO_4{\cdot}7H_2O$ was added under stirring at 80 °C until the mixture became uniform, which was then aged at 90 °C overnight and calcined at 580 °C for 2 h to obtain $ZnSnO_3$ NCs.

DAM NPs were synthesized following the previous report [23]. 2 mL of concentrated ammonia, 40 mL of ethyl alcohol and 90 mL of ultrapure water were mixed and stirred for half an hour. Then, 50 mg/mL of dopamine hydrochloride (10 mL) was added to the solution. During stirring, the color of the mixture become from yellow to brown. After stirring for another 24 h, the precipitate was centrifuged and washed with water to obtain DAM NPs.

2.3. Preparation of DAM-AAO@Ab_2

The loading of AAO and Ab_2 on DAM NPs was performed by adding 1 mg AAO and 2 mL PBS containing 10 μg/mL *anti*-NSE antibody (Ab_2) in the mixture of 1 mL dispersion of DAM NPs and 50 μL of EDC (5 mg/mL) and NHS (1 mg/mL) to vibrate at 37 °C for 6 h. After centrifuged at 4500 r, the product was dispersed in 2 mL PBS, and was then added with 100 μL of BSA (1 wt%) to block the active sites by shacking at 37 °C for another 1 h. The obtained DAM-AAO@Ab_2 was finally redispersed in 2 mL of PBS after centrifugation, and stored at 4 °C refrigerator for the following use.

2.4. Construction of PEC immunosensor

After the ITO glass was washed with ultrapure water, 10 μL of $ZnSnO_3$ NCs dispersion (6 mg/mL) was dropped on its surface (Scheme 1). The BiOI NAs were then modified on ITO/$ZnSnO_3$ NCs by SILAR, which was performed by immersing ITO/$ZnSnO_3$ NCs in 5 mmol/L $Bi(NO)_3$ and 5 mmol/L KI for 10 s respectively, and rinsing with ultrapure water after each soak. This process was repeated for 20 times to obtain ITO/$ZnSnO_3$ NCs/BiOI NAs, which was placed in a muffle furnace at 200 °C to calcine for 2 h. The ITO/BiOI NAs was prepared with the same procedure by using ITO glass. The PDA was then formed on ITO/$ZnSnO_3$

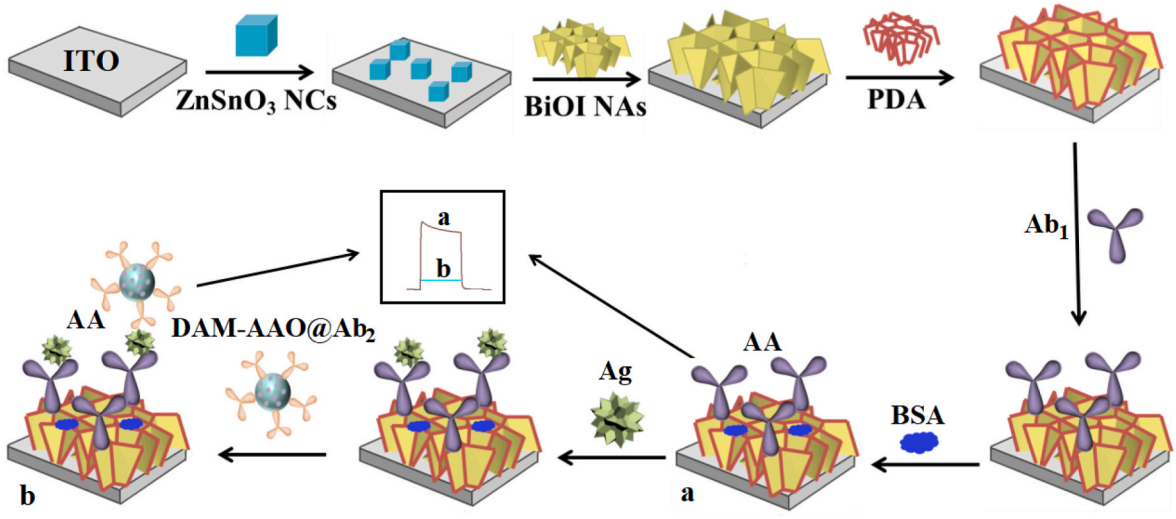

Scheme 1. Schematic illustration for preparation of PEC immunosensor and immunoassay.

NCs/BiOI NAs by self-oxidation polymerization of dopamine, which was carried out by immersing the ITO/$ZnSnO_3$ NCs/BiOI NAs in air-saturated tris-HCl (pH 8.5, 0.5 mol/L) containing 3 mg/mL dopamine hydrochloride for 60 min [19]. The quinone groups of PDA could couple with amine-terminated biomolecules by Michael reaction. After washed carefully with water, 4 μL of Ab_1 (5 μg/mL) was incubated on the obtained ITO/$ZnSnO_3$ NCs/BiOI NAs/PDA at 37 °C for 2 h. The unbound Ab_1 was removed by washing with PBS, and the left active sites were blocked with 3 μL BSA (1 wt %) at 37 °C for 1 h. The obtained ITO/$ZnSnO_3$ NCs/BiOI NAs/PDA/Ab_1/BSA as the PEC immunosensor was stored at 4 °C for further immunoassay.

2.5. PEC immunoassay

After 6 μL of NSE at various concentrations were incubated on the immunosensors for at 37 °C 1 h, 6 μL of DAM-AAO@Ab_2 was dropped on the surface to incubate at 37 °C for another 1 h, which was then washed with 0.1 mol/L PBS (pH 7.4) to perform the PEC measurement with 100 W LED lamp in the 0.1 mol/L PBS (pH 7.4) containing 0.1 mol/L AA using the immunosensor as working electrode. The applied voltage was 0 V.

3. Results and discussion

3.1. Materials characterization

The crystalline phases of prepared materials were characterized with X-ray diffraction (XRD). $ZnSnO_3$ precursor displayed the peaks at 22.98°, 32.57°, 40.12°, 46.70°, 52.78° and 58.24° corresponding to (200), (220), (222), (400), (024) and (422) (JCPDS 74–1825) (Fig. 1A,

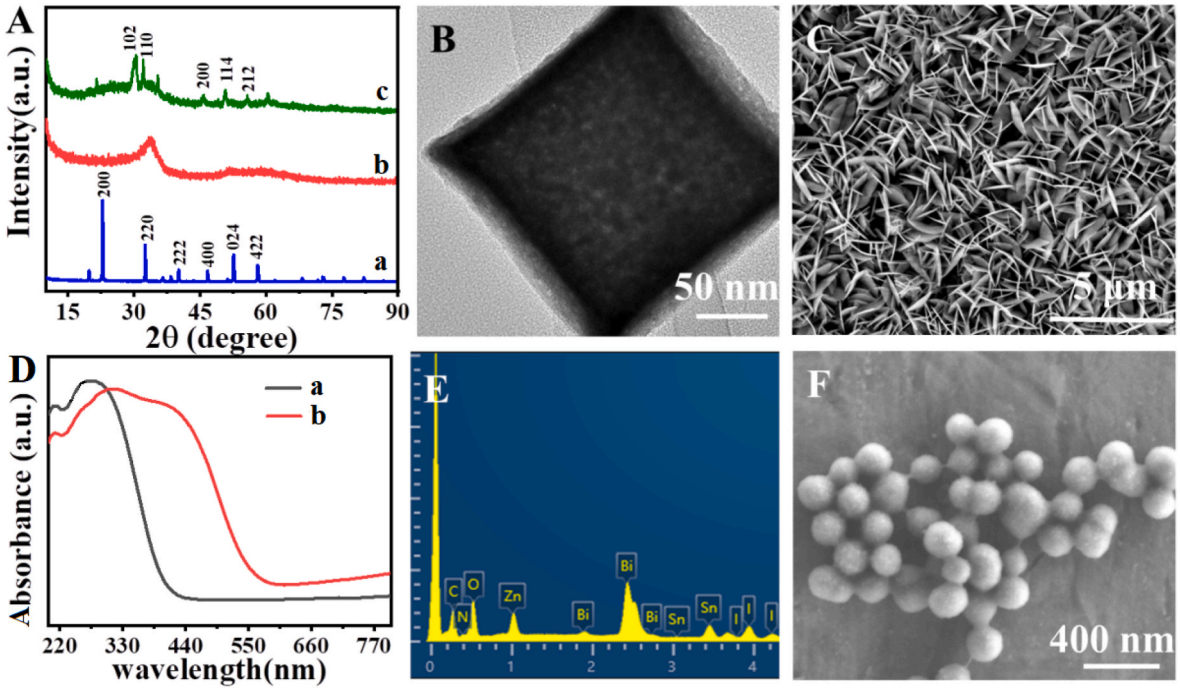

Fig. 1. (A) XRD spectra of $ZnSnO_3$ precursor, $ZnSnO_3$ NCs and $ZnSnO_3$ NCs/BiOI NAs. (B) TEM image of $ZnSnO_3$ NCs. (C) SEM image of $ZnSnO_3$ NCs/BiOI NAs. (D) UV–vis spectra of $ZnSnO_3$ NCs and $ZnSnO_3$ NCs/BiOI NAs. (E) EDS spectrum of $ZnSnO_3$ NCs/BiOI NAs/PDA film. (F) SEM image of DAM.

a). After calcination, the precursor became amorphous $ZnSnO_3$ NCs (Fig. 1B) without any diffraction lines corresponding to crystals (Fig. 1A and b) [15]. After BiOI NAs were grown on ITO/$ZnSnO_3$ NCs by SILAR, the XRD spectrum showed the significant peaks at 29.65°, 31.65°, 45.38°, 51.35° and 55.15°, which belonged to (102), (110), (200), (114) and (212) crystallographic plane of BiOI NAs (JCPDS 04–0477) (Fig. 1A, c). The size of about 200 nm for $ZnSnO_3$ NCs (Fig. 1B) was benefit for the grown of BiOI with sheet nanoarrays (Fig. 1C). The growth of BiOI NAs on $ZnSnO_3$ NCs extended the light absorption range to the visible light (Fig. 1D), and thus greatly improved the utilization of light irradiation. In addition, the energy dispersive spectrum of $ZnSnO_3$ NCs/BiOI NAs/PDA demonstrated the elemental composition of Zn, Sn, O, Bi, I, C and N elements.

X-ray photoelectron spectroscopic (XPS) analysis was further used to verify the preparation of $ZnSnO_3$ NCs/BiOI NAs, which showed the existence of O, Bi, I, Sn and Zn (Fig. 2A). The high-resolution XPS spectrum of O 1s exhibited three peaks at about 529.8, 530.6 and 531.9 eV, which were assigned respectively to the bond between O^{2-} and Sn/Zn oxygen vacancy surface regions, and the weak binding of –OH or $–CO_3$ [14]. The Zn 2p spectrum gave the binding energy of about 1021.65 eV for Zn 2p3/2 and 1044.9 eV for Zn 2p1/2 (Fig. 2C) [24]. The Sn 3d spectrum showed two peaks at 495.1 and 486.8 eV (Fig. 2C), which were the binding energy of Sn 3d3/2 and Sn 3d5/2, respectively [25]. The binding energy located at 618.9 and 630.4 eV was correspond to I 3d5/2 and I 3d3/2, respectively [26]. The two peaks of Bi4f at 158.9 and 164.2 eV were assigned to Bi 4f7/2 and Bi 4f5/2 respectively (Fig. 2F) [27].

3.2. Characterization of PEC immunosensor

After $ZnSnO_3$ NCs was cast on ITO glass, a weak photocurrent was observed in 0.1 mol/L PBS (pH 7.4) containing 0.1 mol/L AA, while bare ITO did not show the photocurrent response (Fig. 3A, curves a and b). The casting of $ZnSnO_3$ NCs also resulted in the increase of electron transfer resistance (Fig. 3B, curves a and b). After BiOI NAs were grown on the ITO/$ZnSnO_3$ NCs, the photocurrent increased sharply, though the electron transfer resistance also further increased due to the low conductivity of semiconductor materials (Fig. 3A and B, curve c), indicating the sensitization of BiOI NAs to the photocurrent response of $ZnSnO_3$ NCs owing to the narrow and matching band gap of BiOI NAs with that of $ZnSnO_3$ NCs. After PDA film was deposited on ITO/$ZnSnO_3$ NCs/BiOI NAs, the photocurrent continued to enhance (Fig. 3A, curve d), which resulted from the facts that PDA could promote the photo-generated e^-/h^- separation of the semiconductors, and increased the photo-electron conversion efficiency [28]. Interestingly, the presence of PDA decreased electron transfer resistance of ITO/$ZnSnO_3$ NCs/BiOI NAs (Fig. 3B, curve d), which should be attributed to the positive charge of PDA due to its $–NH_2$ group, and thus accelerated the electron transfer of anion probes and electron donor AA. After ITO/$ZnSnO_3$ NCs/BiOI NAs/PDA was modified with Ab_1 and then BSA, and the immunosensor captured the target protein, the photocurrent successively decreased (Fig. 3A, curves e-g), which could be attributed to the hindrance of insulating protein molecules to the electron transfer (Fig. 3B, curves e-g) [8]. These phenomena proved the successful construction of the PEC immunosensor and its recognition to the target protein.

The prepared DAM showed well spherical shape with a size of about 160 nm (Fig. 1F). After AAO and Ab_2 co-immobilized on DAM NPs, the formed DAM-AAO@Ab_2 could be recognized by immunosensor/NSE to form a sandwich-type immunocomplex, which increased the electron transfer resistance (Fig. 3B, curve h). It is noteworthy that the decrease of photocurrent due to the introduction of DAM-AAO@Ab_2 onto immunosensor/NSE surface was much greater than the change resulted from the loading of Ab_1 and the capture of NSE, implying a new photocurrent quenching mechanism described as fellows.

The band gaps of $ZnSnO_3$ NCs and BiOI NAs could be obtained from UV–vis diffuse reflectance spectra to be 3.42 and 1.93 eV, respectively (Fig. 4). $ZnSnO_3$ NCs had a large band gap and thus showed a small photoelectric effect (Fig. 3C). The grown BiOI NAs with a relatively narrow band gap served as an energy level matching structure to sensitize $ZnSnO_3$ NCs, thus produced large PEC signal. Under the light irradiation, the electron transition from the valence band (VB) to the conduction band (CB) occurred in $ZnSnO_3$ NCs and BiOI NAs [29,30]. Since the band gap of BiOI NAs was more narrow, the electron transition was easier. Moreover, the electron could be injected to the hole of $ZnSnO_3$ NCs due to its low energy level of valence band, which promoted the electron transition of $ZnSnO_3$ NCs, led to more electron transferred to ITO electrode, and thus sensitized the photocurrent. The formed hole of BiOI NAs could be removed by oxidizing near AA molecule as the electron donor to maintain the photocurrent signal. PDA film not only promoted the electron transfer, but also improved the photo-electron conversion efficiency, thus further increased the photocurrent. The photocurrent quenching after DAM-AAO@Ab_2 was captured onto immunosensor could be attributed to both the competitive consumption of surface AA through the AAO catalyzed oxidation by dissolved oxygen, and the light absorption of DAM [29,30]. The dual quenching effect was beneficial to improve the sensitivity of the "On-Off" immunoassay.

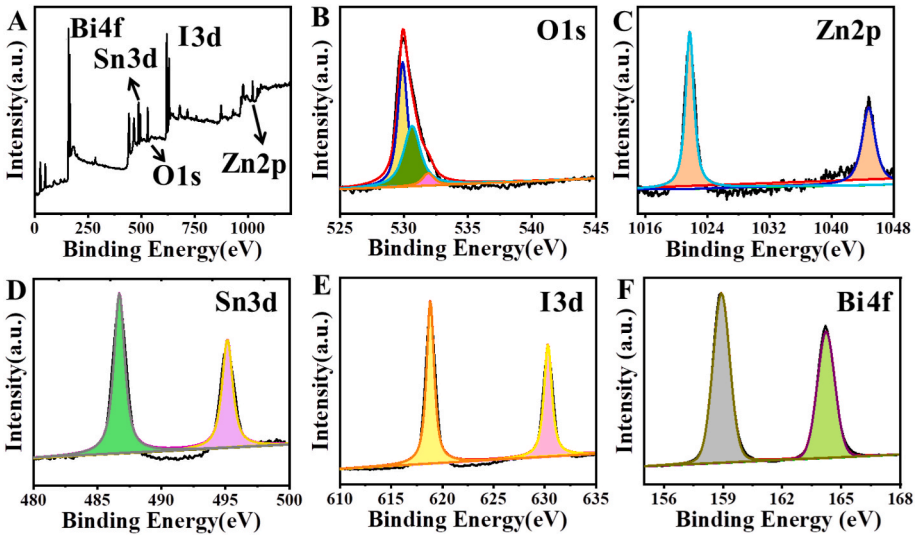

Fig. 2. (A) Full-survey XPS spectrum of $ZnSnO_3$ NCs/BiOI NAs. (B–F) High-solution XPS spectra of O1s (B), Zn2p (C), Sn3d (D), I3d (E) and Bi 4f (F).

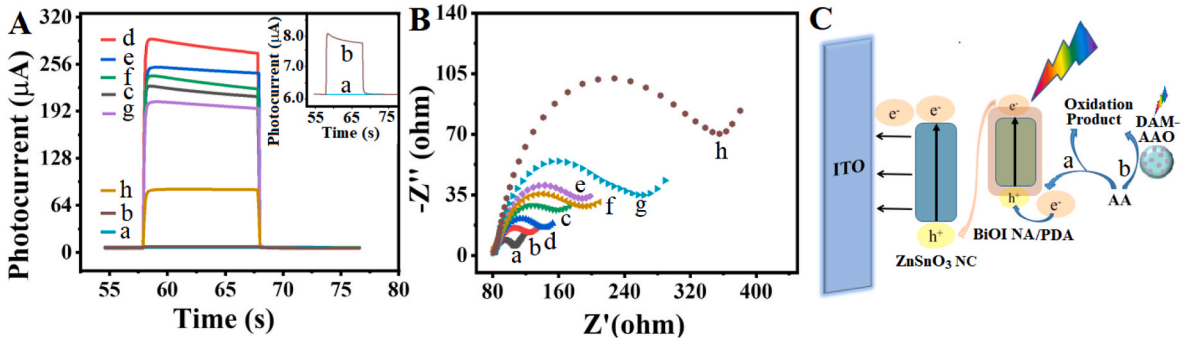

Fig. 3. (A) Photocurrent responses and (B) EIS characterization of ITO (a), ITO/$ZnSnO_3$ NCs (b), ITO/$ZnSnO_3$ NCs/BiOI NAs (c), ITO/$ZnSnO_3$ NCs/BiOI NAs/PDA (d), ITO/$ZnSnO_3$ NCs/BiOI NAs/PDA/Ab_1(e), immunosensor (f), immunosensor/NSE (g), immunosensor/NSE/DAM-AAO@Ab_2 (h) in 0.1 mol/L PBS (pH 7.4) containing 0.1 mol/L AA and 0.1 mol/L KCl containing 2.5 mmol/L $Fe(CN)_6^{3-/4-}$, respectively. (C) Possible mechanism of the proposed PEC immunosensor. Inset in (A): Enlarge of (a) photocurrent responses at ITO and (b) ITO/$ZnSnO_3$ NCs.

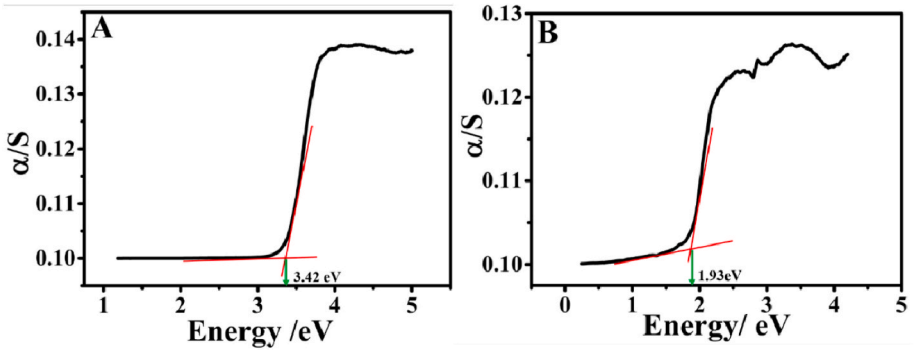

Fig. 4. Kubelka-Munk energy curves of (A) $ZnSnO_3$ NCs and (B) BiOI NAs from UV–vis diffuse reflectance spectra.

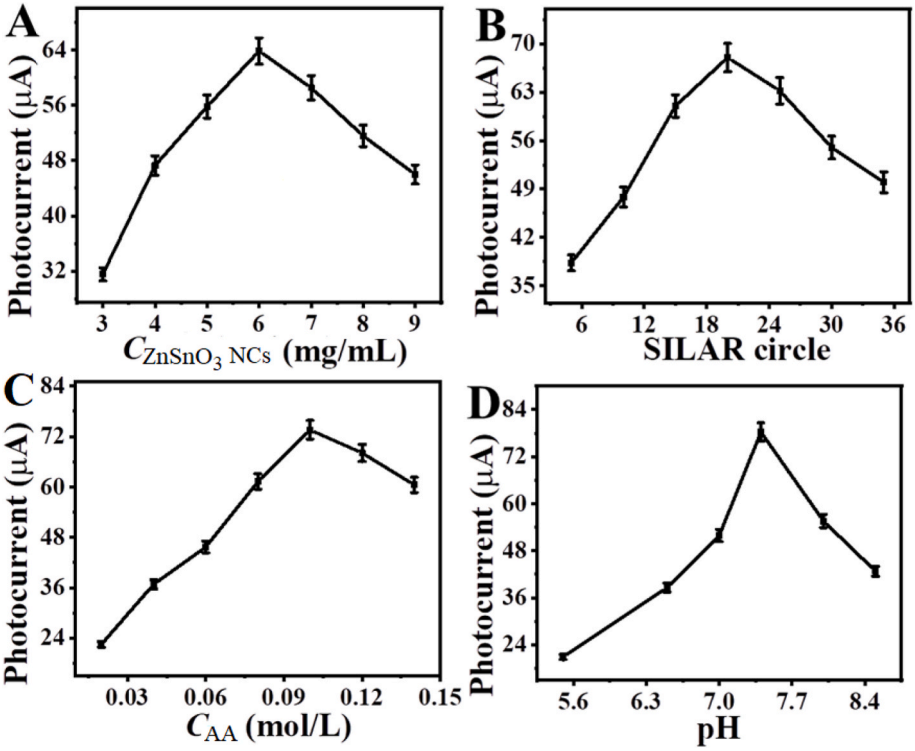

Fig. 5. Optimization of (A) concentration of $ZnSnO_3$ NCs for preparation of immunosensor, (B) cycle number of immersion for forming BiOI NAs, (C) AA concentration and (D) pH of detection solution for PEC test. When one condition changed, the others were at their optimal values.

3.3. Condition optimization for PEC detection

To achieve the best performance of the immunoassay method, some key conditions such as the amount of $ZnSnO_3$ NCs and the SILAR cycle number to grow BiOI NAs for preparation of PEC immunosensor, the concentration of AA and the pH of detection solution were optimized. The photocurrent increased with the increasing amount of $ZnSnO_3$ NCs and reached the maximum value at 6 mg/mL (Fig. 5A). More $ZnSnO_3$ NCs hindered the electron cycle number of SILAR and showed the maximum value at 20 cycles (Fig. 5B), at which the obtained ITO/$ZnSnO_3$ NCs/BiOI NAs/PDA provided the best matrix for preparation of the immunosensors. AA as an electron donor inhabited the recombination of photogenerated e^-/h^+,

and thus increased the photocurrent response [31,32]. When the detection solution contained 0.1 mol/L AA, the photocurrent arrived at the maximum value (Fig. 5C). Because H^+ participated in the oxidation reaction of AA, pH of detection solution also affected the performance of PEC immunosensor, and the optimal pH should be 7.4 (Fig. 5D). Thus pH 7.4 PBS containing 0.1 mol/L AA was used for following PEC immunoassay.

3.4. Performance of PEC immunoassay

Under the optimal conditions, the immunosensor showed sensitive response to NSE. As shown in Fig. 6A, the photocurrent decreased with the increasing NSE concentration due to the sandwich-type capture of more DAM-AAO@Ab_2 by the immunosensor. The plot of photocurrent vs the logarithm of NSE concentration showed a linearity with a slope of −15.8 μA/order of magnitude in the range of 0.1 pg/mL ~50 ng/mL (Fig. 6B). The limit of detection for NSE was 0.03 pg/mL (S/N = 3). Both the detectable concentration range and the limit of detection for NSE were better than those of other electrochemical immunosensors for NSE detection (Table 1).

The proposed immunosensor for NSE showed good selectivity when it was used for the immunoassay of NSE samples containing different interfering substances such as procalcitonin (PCT), amino-terminal pro-B-type natriuretic peptide (NT-pro BNP), prostate-specific antigen (PSA), β-Amyloid oligomers (Aβ) and insulin. At the concentration of 50 times NSE, these interfering substances did not significantly affect the response signal of the immunosensor to 1 ng/mL NSE (Fig. 6C).

Table 1
Comparison of the developed PEC immunosensor with other electrochemical immunosensors for detecting NSE.

Method	Linear range (ng/mL)	Detection limit (pg/mL)	Reference
Impedimetric immunosensor	0.0002–0.0075	0.0061	[37]
Microfluidic paper-based electrochemical measurement	1–500	10	[38]
Electrochemical sensor	0.0001–100	0.483	[39]
Electrochemical sensor	1–1000	300	[40]
Electrochemiluminescent immunoassay	0.0002–20	0.079	[41]
Photoelectrochemical sensor	0.005–200	1.2	[42]
This work	0.0001–50	0.03	This work

The detection stability of the suggested immunosensor was examined via recording the photocurrent with on/off light irradiation cycle with an interval of 10 s [33,34], which showed the satisfactory stability for continous measurments (Fig. 6D). The immunosensor also showed acceptable storage stability, and could remind more than 90% initial response after storage for two weeks (Fig. 6E). Five PEC immunosensors prepared with an identical ITO glass slide were used to examine the repeatability [35,36]. The relative standard deviation (RSD) at 1 ng/mL NSE was 2.82%, implying the excellent repeatability of the proposed PEC immunosensors (Fig. 6F).

3.5. Immunoassay of NSE in practical samples

The practicability of the proposed dual quenching strategy and immunosensing method was examined by adding 2.0, 5.0 and 10.0 nL/mL of NSE to real serum samples. The detection results were listed in Table 2. The average NSE concentrations in the samples were obtained to be 3.66 and 19.22 ng/mL. The recoveries were in the range of 97.5%–104.9%, and the RSDs were between 1.8 and 4.5%, proving the good accuracy and feasibility of the PEC immunosensing method. Thus this

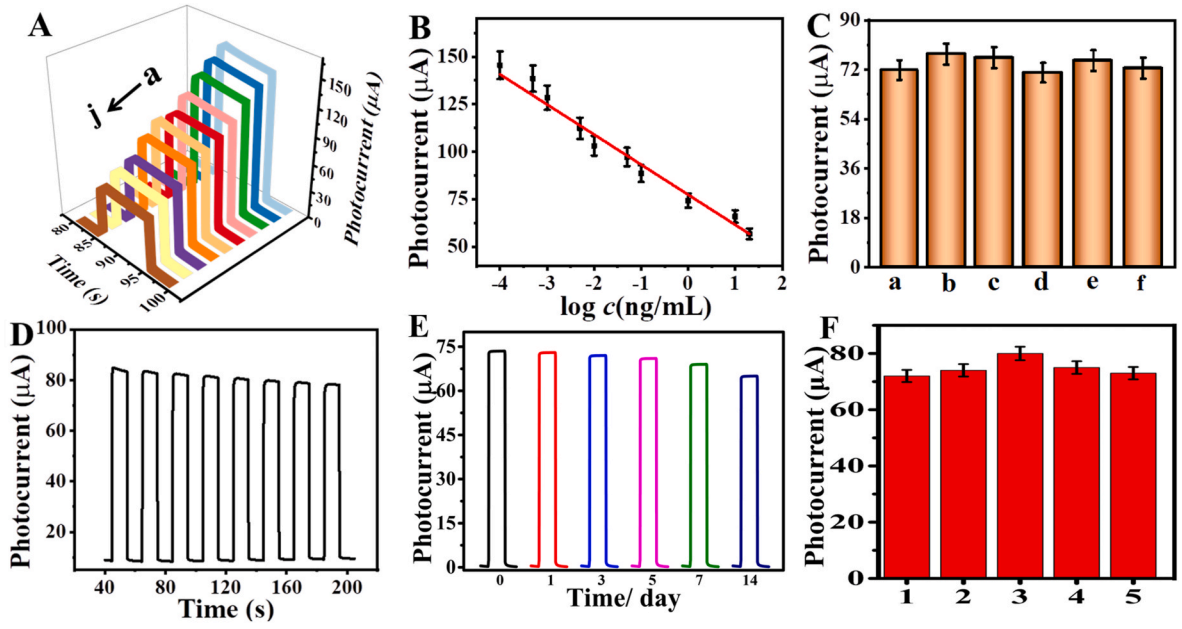

Fig. 6. (A) Photocurrent response curves at 0.1 (a), 1.0 (b), 10 pg/mL (c), and 0.1 (d), 0.5 (e), 1.0 (f), 10 (g) and 50 ng/mL (h) of NSE. (B) Plot of photocurrent vs logarithm of NSE concentration. (C) Photocurrents of PEC immunosensor for NSE at 1.0 ng/mL NSE (a), and (a) + 50 ng/mL PCT (b), NT-pro BNP (c), PSA (d), Aβ (e) and insulin (f). (D) Stability of the proposed PEC immunosensor for continous measurments at 1.0 ng/mL NSE. (E) Storage stability of the PEC immunosensors. (F) Repeatability of five PEC immunosensors at 1.0 ng/mL NSE.

Table 2
NSE detection in human serum samples.

Samples (ng/mL)	Added amount (ng/mL)	Average measured value (ng/mL, $n = 11$)	Average obtained value (ng/mL, $n = 11$)	RSD (%)	Recovery (%)
3.66	2.00	5.61	1.95	1.8	97.5
	5.00	8.58	4.92	2.6	98.4
	10.00	13.82	10.16	3.8	101.6
19.22	2.00	21.19	1.97	2.2	98.5
	5.00	24.34	5.12	3.7	102.4
	10.00	29.71	10.49	4.5	104.9

work provided a promising strategy for sensitive immunoassay of protein biomarkers and clinical early diagnosis.

4. Conclusion

A competitive consumption strategy of surface electron donor and light absorption for quenching the photocurrent has been designed. The well matching structure of band gaps between $ZnSnO_3$ NCs and BiOI NAs, the excellent light absorption ability of BiOI NAs with relatively narrow band gap, and the high photo-electron conversion efficiency of PDA as well as the accelerated electron transfer result in strong photocurrent response in the presence of AA as an electron donor. After capture antibody is bound to ITO/$ZnSnO_3$ NCs/BiOI NAs/PDA, the prepared immunosensor shows specific recognition to corresponding target, and the introduced DAM-AAO@Ab_2 can competitively consume surface AA through the enzymatic oxidation and the light irradiation through the absorption of DAM, which sensitively quenches the photocurrent, and thus provides a sensitive sandwich-type PEC immunosensing method for target detection. The proposed immunosensor for NSE shows excellent performance with a limit of detection of 0.03 pg/mL and good accuracy for practical sample analysis, which demonstrates the practicability of the proposed dual quenching strategy with the designer label. This work provides a good opportunity for the development of labelling immunoassay and the detection of protein biomarkers in clinic samples.

CRediT authorship contribution statement

Yu Du: Conceptualization, Data curation, Investigation, Writing – original draft. **Siqi Yu:** Methodology, Formal analysis, Data curation. **Zhaohui Li:** Methodology, Formal analysis, Writing – review & editing. **Huangxian Ju:** Supervision, Funding acquisition, Project administration, Writing – review & editing.

Declaration of competing interest

The authors declare that they have no known competing financial interests or personal relationships that could have appeared to influence the work reported in this paper.

Acknowledgements

This study was supported by the National Natural Science Foundation of China (Nos. 21890741, 21827812), Jinan Scientific Research Leader Workshop Project (2018GXRC024).

References

[1] Q. Han, X. Zhao, N. Na, J. Ouyang, Integrating near-infrared visual fluorescence with a photoelectrochemical sensing system for dual readout detection of biomolecules, Anal. Chem. 93 (2021) 3486–3492.
[2] Y. Bai, H. Bai, Z. Fang, X. Li, W. Fan, W. Shi, Understanding the Z-scheme heterojunction of BiVO4/PANI for photoelectrochemical nitrogen reduction, Chem. Commun. 57 (2021) 10568–10571.
[3] B. Zhang, Y. Tang, X. Wu, H. Xie, F. Zhao, B. Zeng, Experimental and DFT studies of novel Z-scheme Bi-doped Bi2WO6/Bi2S3 p-n/n homo/heterojunction and its application in cathodic photoelectrochemical immunosensing, Sens. Actuators B-Chem. 346 (2021), 130455.
[4] R. Xu, Y. Du, H. Ma, D. Wu, X. Ren, X. Sun, Q. Wei, H. Ju, Photoelectrochemical aptasensor based on $La_2Ti_2O_7/Sb_2S_3$ and V_2O_5 for effectively signal change strategy for cancer marker detection, Biosens. Bioelectron. 192 (2021), 113528.
[5] W. Tu, W. Wang, J. Lei, S. Deng, H. Ju, Chemiluminescence excited photoelectrochemistry using graphene-quantum dots nanocomposite for biosensing, Chem. Commun. 48 (2012) 6535–6537.
[6] G. Wen, H. Ju, Enhanced photoelectrochemical proximity assay for highly selective protein detection in biological matrixes, Anal. Chem. 88 (2016) 8339–8345.
[7] R. Xu, L. Liu, X. Liu, Y. Li, R. Feng, H. Wang, D. Fan, D. Wu, Q. Wei, Novel electron donor encapsulation assay based on the split-type photoelectrochemical interface, ACS Appl. Mater. Interfaces 12 (2020) 7366–7371.
[8] R. Xu, Y. Du, D. Leng, L. Liu, Y. Li, X. Ren, D. Fan, H. Wang, Q. Wei, Antigen down format photoelectrochemical analysis supported by fullerene functionalized Sn_3O_4, Chem. Commun. 56 (2020) 7455–7458.
[9] Y.X. Dong, J.T. Cao, Y.M. Liu, S.H. Ma, A novel immunosensing platform for highly sensitive prostate specific antigen detection based on dual-quenching of photocurrent from CdSe sensitized TiO_2 electrode by gold nanoparticles decorated polydopamine nanospheres, Biosens. Bioelectron. 91 (2017) 246–252.
[10] R. Xu, D. Wei, B. Du, W. Cao, D. Fan, Y. Zhang, Q. Wei, H. Ju, A photoelectrochemical sensor for highly sensitive detection of amyloid beta based on sensitization of Mn:CdSe to Bi_2WO_6/CdS, Biosens. Bioelectron. 122 (2018) 37–42.
[11] A. Biswas, S. Saha, N.R. Jana, $ZnSnO_3$ nanoparticle-based piezocatalysts for ultrasound-assisted degradation of organic pollutants, ACS Appl. Nano Mater. 2 (2019) 1120–1128.
[12] G. Feng, Y. Che, C. Song, J. Xiao, X. Fan, S. Sun, G. Huang, Y. Ma, Morphology-controlled synthesis of $ZnSnO_3$ hollow spheres and their n-butanol gas-sensing performance, Ceram. Int. 47 (2021) 2471–2482.
[13] R. Guo, Y. Guo, H. Duan, H. Li, H. Liu, Synthesis of orthorhombic perovskite-Type $ZnSnO_3$ single-crystal nanoplates and their application in energy harvesting, ACS Appl. Mater. Interfaces 9 (2017) 8271–8279.
[14] P. Luo, H. Zhang, L. Liu, L. Fang, Y. Wang, Sandwich-like nanostructure of amorphous $ZnSnO_3$ encapsulated in carbon nanosheets for enhanced lithium storage, Electrochim. Acta 219 (2016) 734–741.
[15] J. Huang, X. Xu, C. Gu, W. Wang, B. Geng, Y. Sun, J. Liu, Size-controlled synthesis of porous $ZnSnO_3$ cubes and their gas-sensing and photocatalysis properties, Sens. Actuators B-Chem. 171–172 (2012) 572–579.
[16] J. Xue, W. Cheng, L. Shi, Y. Li, M. Sheng, Y. Shi, Q. Bi, BiOI/carbon aerogel composite photoanode with enhanced adsorption and solar-driven photoelectrocatalytic properties, Appl. Surf. Sci. 571 (2022), 151325.
[17] A.M. Chang, Y.H. Chen, C.C. Lai, Y.C. Pu, Synergistic effects of surface passivation and charge separation to improve photo-electrochemical performance of BiOI nanoflakes by Au nanoparticle decoration, ACS Appl. Mater. Interfaces 13 (2021) 5721–5730.
[18] H. Ben, Y. Liu, X. Liu, X. Liu, C. Ling, C. Liang, Diffusion-controlled Z-scheme-steered charge separation across PDI/BiOI heterointerface for ultraviolet, visible, and infrared light-driven photocatalysis, Adv. Funct. Mater. 31 (2021), 2102315.
[19] C. Bao, D. Fan, X. Liu, X. Wang, D. Wu, H. Ma, H. Wang, X. Sun, Q. Wei, A signal-off type photoelectrochemical immunosensor for the ultrasensitive detection of procalcitonin: $Ru(bpy)_3(2+)$ and Bi_2S_3 co-sensitized $ZnTiO_3/TiO_2$ polyhedra as matrix and dual inhibition by SiO_2/PDA-Au, Biosens. Bioelectron. 142 (2019), 111513.
[20] Q. Xiong, Q. Fang, K. Xu, G. Liu, M. Sang, Y. Xu, L. Hao, S. Xuan, Near-infrared light-responsive photothermal alpha-Fe_2O_3@Au/PDA core/shell nanostructure with on-off controllable anti-bacterial effects, Dalton Trans. 50 (2021) 14235–14243.
[21] Y.-M. Liu, J.-J. Zhang, G.-F. Shi, M. Zhou, Y.-Y. Liu, K.-J. Huang, Y.H. Chen, Label-free electrochemiluminescence aptasensor using $Ru(bpy)_3^{2+}$ functionalized dopamine-melanin colloidal nanospheres and gold nanoparticles as signal-amplifying tags, Electrochim. Acta 129 (2014) 222–228.
[22] C.M. Xu, Y.L. Luo, S. Li, Z.X. Li, L. Jiang, G.X. Zhang, L. Owusu, H.L. Chen, Multifunctional neuron-specific enolase: its role in lung diseases, Biosci. Rep. 39 (2019), BSR20192732.
[23] Y. Liu, K. Ai, J. Liu, M. Deng, Y. He, L. Lu, Dopamine-melanin colloidal nanospheres: an efficient near-infrared photothermal therapeutic agent for in vivo cancer therapy, Adv. Mater. 25 (2013) 1353–1359.
[24] M.u. Haq, Z. Zhang, X. Chen, N. Rahman, S. Khan, R. Khatoon, S.S. Hassan, Z. Ye, L. Zhu, A two-step synthesis of microsphere-decorated fibers based on NiO/$ZnSnO_3$ composites towards superior ethanol sensitivity performance, J. Alloys Compd. 777 (2019) 73–83.
[25] T. Zhou, T. Zhang, R. Zhang, Z. Lou, J. Deng, L. Wang, Hollow $ZnSnO_3$ cubes with controllable shells enabling highly efficient chemical sensing detection of formaldehyde vapors, ACS Appl. Mater. Interfaces 9 (2017) 14525–14533.
[26] J. Niu, P. Dai, Q. Zhang, B. Yao, X. Yu, Microwave-assisted solvothermal synthesis of novel hierarchical BiOI/rGO composites for efficient photocatalytic degradation of organic pollutants, Appl. Surf. Sci. 430 (2018) 165–175.
[27] X. Hu, G. Wang, J. Wang, Z. Hu, Y. Su, Step-scheme NiO/BiOI heterojunction photocatalyst for rhodamine photodegradation, Appl. Surf. Sci. 511 (2020), 145499.
[28] R. Xu, K. Xu, Y. Du, J. Li, L. Dai, T. Wu, X. Ren, Q. Wei, Peptide-based antifouling photoelectrochemical interface for NSE sensitive detection, Sens. Actuators B-Chem. 361 (2022), 131702.

[29] R. Zeng, H. Gong, Y. Li, Y. Li, W. Lin, D. Tang, K. Dietmar, CRISPR-Cas12a-derived photoelectrochemical biosensor for point-of-care diagnosis of nucleic acid, Anal. Chem. 94 (2022), 7442-7428.
[30] Y. Gao, Y. Zeng, X. Liu, D. Tang, Liposome-mediated in situ formation of type-I heterojunction for amplified photoelectrochemical immunoassay, Anal. Chem. 94 (2022) 4859–4865.
[31] K. Zhang, S. Lv, Z. Lin, M. Li, D. Tang, Bio-bar-code-based photoelectrochemical immunoassay for sensitive detection of prostate-specific antigen using rolling circle amplification and enzymatic biocatalytic precipitation, Biosens. Bioelectron. 101 (2018) 159–166.
[32] K. Zhang, S. Lv, Q. Zhou, D. Tang, CoOOH nanosheets-coated g-C_3N_4/$CuInS_2$ nanohybrids for photoelectrochemical biosensor of carcinoembryonic antigen coupling hybridization chain reaction with etching reaction, Sens. Actuators B-Chem. 307 (2020), 127631.
[33] X. Zhong, M. Zhang, L. Guo, Y. Xie, R. Luo, W. Chen, F. Cheng, L. Wang, A dual-signal self-checking photoelectrochemical immunosensor based on the sole composite of MIL-101(Cr) and CdSe quantum dots for the detection of alpha-fetoprotein, Biosens. Bioelectron. 189 (2021), 113389.
[34] J. Ding, Y. Zhou, Q. Wang, S. Ai, Photoelectrochemical biosensor for DNA hydroxymethylation detection based on the enhanced photoactivity of in-situ synthesized Bi_4NbO_8Cl@Bi_2S_3 heterojunction, Biosens. Bioelectron. 194 (2021), 113580.
[35] H. Li, Y. Li, X. Zhang, P. Liu, M. He, C. Li, Y. Wang, Near-infrared photoactive Yb-MOF functionalized with a large conjugate ionic liquid: synthesis and application for photoelectrochemical immunosensing of carcinoma embryonic antigen, Nanoscale 13 (2021) 9757–9765.
[36] D. Chen, X. Zou, F. Dong, C. Zhen, D. Xiao, X. Wang, Donor-acceptor compensated ZnO semiconductor for photoelectrochemical biosensors, ACS Appl. Mater. Interfaces 13 (2021) 33006–33014.
[37] E.B. Aydın, M. Aydın, M.K. Sezgintürk, Selective and ultrasensitive electrochemical immunosensing of NSE cancer biomarker in human serum using epoxy-substituted poly(pyrrole) polymer modified disposable ITO electrode, Sens. Actuators B-Chem. 306 (2020), 127613.
[38] Y. Fan, J. Liu, Y. Wang, J. Luo, H. Xu, S. Xu, X. Cai, A wireless point-of-care testing system for the detection of neuron-specific enolase with microfluidic paper-based analytical devices, Biosens. Bioelectron. 95 (2017) 60–66.
[39] S. Yin, L. Zhao, Z. Ma, Label-free electrochemical immunosensor for ultrasensitive detection of neuron-specific enolase based on enzyme-free catalytic amplification, Anal. Bioanal. Chem. 410 (2018) 1279–1286.
[40] J. Amani, M. Maleki, A. Khoshroo, A. Sobhani-Nasab, M. Rahimi-Nasrabadi, An electrochemical immunosensor based on poly p-phenylenediamine and graphene nanocomposite for detection of neuron-specific enolase via electrochemically amplified detection, Anal. Biochem. 548 (2018) 53–59.
[41] G. Mo, X. He, D. Qin, X. Jiang, X. Zheng, B. Deng, A potential-resolved electrochemiluminescence resonance energy transfer strategy for the simultaneous detection of neuron-specific enolase and the cytokeratin 19 fragment, Analyst 146 (2021) 1334–1339.
[42] H. Wang, H. Wang, Y. Li, H. Wang, X. Ren, Q. Wei, D. Wu, Construction of a photoelectrochemical immunosensor based on $CuInS_2$ photocathode and $BiVO_4$/BiOI/Ag_2S photoanode and sensitive detection of NSE, Biosens. Bioelectron. 211 (2022), 114368.